Author(s): Västilä, Kaisa; Järvelä, Juha; Koivusalo, Harri

Title: Flow-vegetation-sediment interaction in a cohesive compound channel

Year: 2015

Version: Post print

Please cite the original version:

This is a post-print version of the article published by American Society of Civil Engineers (ASCE): Västilä, Kaisa; Järvelä, Juha; Koivusalo, Harri. 2015. Flow-vegetation-sediment interaction in a cohesive compound channel. Journal of Hydraulic Engineering, DOI: 10.1061/(ASCE)HY.1943-7900.0001058

Flow-vegetation-sediment interaction in a cohesive compound channel

K. Västilä[1], J. Järvelä[2], H. Koivusalo[3]

Abstract

The purpose of this study was to quantify how vegetation influences the flow and sediment processes relevant for the design and management of environmental compound channels. Therefore, we conducted a two-year field investigation in a cohesive two-stage channel, focusing on the flow resistance and net deposition in five sub-reaches with different floodplain vegetation conditions. In the grassy sub-reaches, the cross-sectional blockage factor was the key vegetation property governing the flow resistance, with a process-based model providing reliable estimates under widely variable hydraulic and vegetative conditions. The net deposition of cohesive sediment was best explained by the vegetation height while high stand length and density created supply-limited conditions on the inner floodplain. Our results showed that the two-stage approach offers potential for controlling the sediment processes through appropriate vegetation maintenance. The novelty of this research was that straightforward analyses accompanied with a physically-based parameterization of the floodplain plant stands were successfully used to characterize the flow–vegetation–sediment interaction in a practical engineering application. The results are expected to be helpful in designing and managing comparable channels.

Subject headings: Flow resistance; Cohesive soils; Suspended sediment; Vegetation; Drainage; Hydraulic models

Introduction

There is a growing interest towards environmentally sound hydraulic engineering, which attempts to combine technical requirements and ecological aspects in the management of rivers, brooks, and drainage channels (e.g., Hey 2009). One of the environmentally preferable alternatives is a two-stage channel, which refers to a compound cross-section with an excavated floodplain on one or both sides of the main channel (e.g., Powell et al. 2007; USDA 2007). The floodplain is typically designed to be annually inundated for several weeks to months. The two-stage approach has been adopted e.g. in agricultural drainage (Powell et al. 2007; Västilä and Järvelä 2011) and flood management (Geerling et al. 2008; Sellin et al. 1990) in an attempt to provide both ecological benefits and improved conveyance of high flows. Another focus is often on the management of in-channel transport processes of fine suspended sediment (SS). High loads of SS can lead to excessive sedimentation, which decreases the conveyance and alters the morphology and habitats

[1]Doctoral student, Dept. of Civil and Environmental Engineering, Aalto University School of Engineering, P.O. Box 15500, FI-00076 Aalto, Finland (corresponding author). Email: kaisa.vastila@aalto.fi
[2]Staff Scientist, Dept. of Civil and Environmental Engineering, Aalto University School of Engineering, P.O. Box 15500, FI-00076 Aalto, Finland.
[3]Professor, Dept. of Civil and Environmental Engineering, Aalto University School of Engineering, P.O. Box 15200, FI-00076 Aalto, Finland.

(e.g., Owens et al. 2005). In addition, the cohesive fraction (<60 μm) conveys sorbed harmful substances (e.g., nutrients, heavy metals, and pesticides) and increases turbidity, affecting benthic and aquatic biota and water quality (e.g., Bilotta and Brazier 2008). Two-stage channels can be aimed at bringing the sediment processes to a state of dynamic equilibrium or at improving the downstream water quality by sediment deposition on the floodplain. Compared to over-wide trapezoidal designs, the compound cross-section is expected to decrease siltation in the main channel by keeping the low flow velocities high enough, which can decrease the need for channel maintenance (Powell et al. 2007; USDA 2007).

Compound channels are hydraulically complex because of the interaction between the main channel and the vegetated floodplain. Thus, their design and management require reliable estimation of how the natural vegetation affects the flow and sediment transport, which is particularly difficult for small channels where individual roughness elements have a larger impact on the total resistance compared to wider and deeper channels. Field studies in two-stage reaches often provide only a cursory description of the vegetation properties (e.g., Helmiö and Järvelä 2004; Myers and Lyness 1994; Sellin et al. 1990). In simple cross-sections with submerged vegetation covering the entire bed, the flow resistance depends primarily on the relative submergence of the plants (Kouwen and Unny 1973; Wu et al. 1999). For patchy aquatic vegetation, empirical equations have been introduced for estimating the flow resistance with bulk vegetative properties, such as the spatially-averaged cross-sectional blockage factor (e.g., Green 2006; Nikora et al. 2008) or the dry mass (e.g., De Doncker et al. 2009). In 1D considerations for compound channels, the total resistance can be obtained by various equations based on partitioning the cross-section (e.g., Yen 2002). However, the resistance coefficient of the floodplain vegetation is typically calibrated, estimated from reference photographs, or known a-priori (e.g., Yang et al. 2014).

Physically-based parameterizations commonly consider the plants as uniformly-spaced rigid cylinders having a specified drag coefficient C_D, frontal area per unit volume a, and stem diameter (e.g., DVWK 1991; Huai et al. 2009; Kang and Choi 2006; Knight et al. 2010). According to Luhar and Nepf (2013), little of the understanding on the flow-vegetation interaction at the patch scale has been applied to the reach scale, suggesting that approaches aimed at practical use need to be straightforward but still use measurable, physically-based vegetative properties. Physically-based formulations that incorporate the reconfiguration properties and the complex structure typical for flexible plant stands have been recently presented for both blade-like aquatic (Luhar and Nepf 2013) and woody vegetation (e.g., Västilä and Järvelä 2014; Jalonen and Järvelä 2014). Overall, the validity of the results obtained with aquatic or simulated plants, and simple channel geometries, needs to be separately assessed for natural floodplain vegetation of compound settings (see e.g., Aberle and Järvelä 2013).

The flow–vegetation interaction has an impact on the transport processes, and it controls the mechanisms of SS supply to the vegetated floodplain. When longitudinal advection is the main supply mechanism, deposition reduces the SS concentration in the downstream direction as the distance from the SS

replenishment point increases (e.g., Zong and Nepf 2011). SS can also be supplied to plant stands via vertical diffusion from the overflow (e.g., Luhar et al. 2008), lateral turbulent diffusion (e.g., Sharpe and James 2006), and lateral advection (e.g., Asselman and Wijngaarden 2002). Luhar et al. (2008) described the transport processes within plant stands in relation to the vegetation-generated modifications in the turbulent flow structure, and characterized the behavior of the stands by the parameter $C_D aH$ where H is the vegetation height. Although deposition on floodplains has been measured (e.g., Kronvang et al. 2009; Walling 1999) and simulated (e.g., Asselman and van Wijngaarden 2002; Walling and He 1997), only few studies have related deposition to measurable vegetation properties (e.g., Corenblit et al. 2009; Thornton et al. 1997). The focus is often on sand-sized sediment while less attention is paid to flocs of cohesive clay and silt that can readily settle on floodplains (e.g., Thonon et al. 2005).

This paper investigates the flow–vegetation–sediment interaction in a cohesive two-stage channel, with the aim of demonstrating how measurable properties of floodplain vegetation can be used to quantify flow resistance, erosion, and deposition in practical applications. For this, we established a field site with floodplain vegetation types ranging from bare soil to grasses and willows. First, we investigate the dependence of the flow resistance on the vegetation properties and evaluate the suitability of a simple, process-based hydraulic model in the two-stage geometry. Second, we examine how the flow–vegetation interaction explained the net deposition and erosion in different parts of the cross-section. Third, we discuss the practical implications of the findings at the reach scale, focusing on the cohesive sediment. Overall, this study seeks to build on the recent theoretical advances to analyze the field data, with the intention of providing help for the design and management of environmental compound channels.

Site and methodology

The experimental two-stage channel

The Ritobäcken Brook in Sipoo, Southern Finland, was channelized in the past to improve the drainage of the surrounding agricultural fields. As an environmentally preferable alternative for enhancing the conveyance of the channel during high flows, a two-stage profile was constructed in February 2010 by excavating an 850 m long floodplain at the level of the estimated mean discharge (described in detail by Västilä and Järvelä 2011). Figs. 1a–b show a representative cross-section comprised of the bank, inner floodplain, 1.2 m wide floodplain–main channel interface, main channel, and the unexcavated bank (hereafter the term floodplain comprises both the inner floodplain and the interface). The mean discharge determined from the site-specific rating curve is 0.12 m^3/s, and the longitudinal bed slope is 0.001–0.002. Agricultural fields comprise 13% of the 10 km^2 catchment area while the remainder is mainly forests and mires. Agricultural fields have mostly clayey soils and form the primary erosion source areas within the catchment (Västilä and Järvelä 2011).

Figure 1. (a) A representative two-stage cross-section with the surveyed geometry in 2010 and 2012; (b) the test reach at a low floodplain water depth; (c) the field site with the monitoring infrastructure.

To investigate how the channel's flow resistance and annual net deposition and erosion depended on selected vegetation properties, we established five 20 m long sub-reaches with differing floodplain vegetation type (Fig. 1c). The sub-reaches labeled as Grasses-D and -U were sown with pasture grasses (mainly *Lolium perenne*), Grasses-N grew naturally established grasses, and Bare-M was intended to have bare soil. Willows-M was planted with cuttings of Common Osier (*Salix viminalis*) at 0.5 m x 0.5 m spacing, and the willows were approximately 1 m tall after two years. Willows-M and Bare-M also had some low ($H \approx 0.05$ m) stubble of grass although the grassy floodplain and bank vegetation of these two reaches was cut in late summer before the period of overbank flows. The sub-reaches were situated close to each other (Fig. 1c),. and had approximately similar geometry: the floodplain width and depth were 3.8–4.6 m and 0.6–0.7 m, respectively, while the bankful wetted area of the main channel was 0.8–1.2 m^2. Hereafter, bankful and overbank refer to the conditions when water level is just below the floodplain level and above the floodplain level, respectively (Fig. 1a). At events with approximately bankful flow, the water level in relation to the floodplain level varied less than 10 cm between the sub-reaches. All sub-reaches had approximately similar vegetation on the unexcavated bank. The areas outside the sub-reaches were allowed to establish a natural grassy vegetation cover. This paper focuses on the two-year period starting from the first summer after the construction in 2010.

Monitoring

This section reports the monitoring conducted at the whole 190 m long vegetated test reach and the five sub-reaches. Continuous monitoring stations were established at the upstream and downstream end of the test reach for recording water levels and turbidity at 5-minute time steps (Fig. 1c, see details below). In addition, the water levels at the upstream and downstream end of each sub-reach were obtained from manual gauge readings during field visits in autumn and spring high flow seasons. The cross-sectional geometry, suspended sediment transport, and the properties of the sediment and vegetation were determined as detailed below.

Cross-sectional surveys

High-resolution surveys were conducted annually in two cross-sections located in the middle of each sub-reach at a 4 m spacing (Fig. 1c) for determining the net erosion and deposition. We used a custom-built framework that was spanned over the cross-section and attached to steel poles hammered to the ground at both ends. The vertical distance from the framework to the ground surface was measured at 0.2–0.4 m horizontal intervals by a point gauge, ensuring that the vegetation did not disturb the measurement. The surveys were conducted in late summer when soil was the driest in order to minimize the impact of soil swelling on the ground elevation. Repeated validation measurements showed that the mean error in the reference level of a single cross-sectional measurement was approximately ± 6 mm. The measurement

system did not allow a reliable estimate of the erosion or deposition on the fluffy, submerged bed of the main channel. The cross-sectional poles and other monitoring infrastructure were geo-referenced annually as part of terrestrial laser scanning campaigns (Jalonen et al. 2014). In the deposition analyses, we used the mean annual values of net deposition and explanatory variables based on the two-year data.

Determination of suspended sediment transport

The suspended sediment transport was determined from the continuous water level and turbidity data that were obtained with pressure transducers and turbidity sensors, respectively, installed in the main channel (Fig. 1c). The detailed procedure of the continuous monitoring, and the data from the downstream station preceding and following the construction were reported by Västilä and Järvelä (2011). The turbidity sensors of the two stations (Analite NEP9530 by McVan Instruments) were identical and calibrated in the laboratory. The cross-sectional representativeness of the turbidity measurements was optimized by positioning the sensors at locations where the flow was most efficiently laterally mixed: the upstream station was located after the sub-reach with the bare floodplain while the downstream station was located in a culvert (Fig. 1c). The sensors were kept at approximately mid-depth by manually changing their vertical position according to the water level.

Water samples were collected in different seasons at turbidity T =20–700 NTU, and suspended sediment concentration (SSC, g/m^3) was analyzed according to the standard EN 872:2005 using GF-52 glass microfibre filters (nominal pore size 1.2 μm) and Nuclepore track-etched polycarbonate membranes (0.4 μm). Separate rating curves were fitted for the 1.2 μm filters (SSC = 0.53T – 3; squared correlation coefficient r^2=0.92, probability p<0.001) and 0.4 μm filters (SSC = 0.59 T + *14*; r^2=0.92, p<0.001). The high correlations indicated that the sensor turbidity provided a reliable estimate of the temporally varying SSC. Annual SS loads were computed by multiplying SSC by the respective discharge (Q) obtained from a rating curve determined at the downstream station (see details in Västilä and Järvelä 2011). For this, we used the turbidity values at the downstream station in the first year and the upstream station in the second year in order to exclude unreliable readings which were easily identifiable in the data. Because the reach between the stations received runoff from an area comprising 2% of the total catchment and having a similar land use as the catchment of the upstream station, equal turbidity values at the stations were assumed to signify that no net erosion or deposition occurred in the test reach. Thus, comparing the turbidity values allowed determining the timing of net deposition and erosion events because the entrained sediment was expected to be transported predominantly in the suspended form.

Sediment properties

The dispersed particle size distribution of the floodplain, bed, and suspended sediment was determined with a laser-based analyzer from samples collected shortly after the end of the monitoring period. The bed sediment of the main channel was sampled with sediment tubes (40 mm in diameter) in each sub-reach.

Composite samples of the top 1 cm layer of the floodplain sediment were taken from the inner floodplain in three sub-reaches, and the samples were ground after incinerating at 550 degrees to remove the organic matter. For the analyses of the bed and floodplain sediment, 1 ml of the sample was mixed with 100 ml of reverse osmosis water. The suspended sediment was analyzed from eight water samples collected at T=120–520 NTU and mixed gently just prior to the analysis. As a pre-treatment, all samples were dispersed by exposing them to ultrasound for 5 minutes. Suspended sediment was also analyzed in the flocculated form without the pre-treatment. Dispersed suspended sediment contained on average 40% of clay (<2 μm) and 60% of silt (2–60 μm). The uppermost 5 cm of the bed sediment contained 11–14% of clay, and 83–97% was comprised of particles finer than 57 μm. The dry bulk density of the floodplain sediment (735 kg/m^3) was determined to compute the deposition mass balance from the cross-sectional and continuous data. The organic content was approximately 10% for the floodplain and bed sediment, and 15–43% for the suspended sediment.

Determination of vegetation properties

Vegetation on the bank, inner floodplain, and interface (Fig. 1a) was sampled annually in late summer when vegetation was the most abundant. Because of the spatial heterogeneity, 3–9 samples were collected from each sub-reach. For the banks having large areas of bare soil, the data were spatially averaged to take into account the vegetation coverage. Grassy vegetation was collected in quadrates of 156 cm^2, photographed in the laboratory, and analyzed for the dry mass m_D. C_DaH was used as a measure of density by employing the commonly assumed value of C_D=1.0 for natural vegetation of similar morphology (e.g., Luhar et al. 2008; Luhar and Nepf 2013). For the vertically heterogeneous grasses, H was defined as the value at which the higher-lying vegetation could be considered as sparse, i.e. having C_DaH=0.1 (Luhar et al. 2008). The total frontal area index aH was determined from nine samples using image analysis techniques, but it was less objective to measure than e.g. dry mass. Thus, the a values were obtained from a fitted linear regression equation without intercept:

$$aH = 6.3m_D \qquad (1)$$

where m_D has the units m^2/kg (r^2=0.86). The vegetation samples were considered to be representative of the entire autumn high flow season because the properties of the grasses remained fairly constant between August and November (see also Jalonen et al. 2014).The grasses that had H≤5 cm in the preceding autumn were assumed to have the same height in the following spring because no bending of such low vegetation was observed. For grasses having H>8 cm, the heights in spring 2011 were assumed to be half of those in the preceding autumn because of bending, while the heights in spring 2012 were determined with terrestrial laser scanning (Jalonen et al. 2014). No sub-reach had $5 < H \leq 8$ cm in autumn.

The properties of the willows were analyzed in both years from the same five specimens considered representative of the height distribution of the stand. The lengths and diameters of the main stem and twigs

were measured in four vertical quartiles to obtain the frontal projected stem area per ground area (A_S/A_B) and the stem volume. H was estimated as the mean height of the specimens, and was assumed to be constant from the late summer to the following spring. The leaves were collected and scanned to obtain the leaf area index (A_L/A_B, where A_L is the total one-sided leaf area and A_B is the corresponding ground area). m_D was derived by summing the foliage dry mass and the stem dry mass estimated from the stem volume and the bulk density of stem samples. The effect of autumnal leaf shedding on m_D was neglected because the foliage comprised <12% of the mass. For the willows, C_DaH was computed as $C_{D\chi,F}A_L/A_B + C_{D\chi,S}A_S/A_B$, where $C_{D\chi,F}$=0.25 and $C_{D\chi,S}$=1.18 correspond to the drag coefficients of the foliage and stem, respectively, at the flow velocity of 0.1 m/s, as derived for the same species from flume measurements (Västilä and Järvelä 2014). In autumn 2011, we also analyzed the wet mass and the vertical structure of the vegetation (such as C_Da in 10-cm layers and the total C_Da at different water depths) in all sub-reaches, and fitted regression equations for interpolating the vegetation properties at intermediate water depths.

In the hydraulic analyses, we used the mean vegetation properties of each sub-reach obtained by spatially averaging the results of the bank, inner floodplain, and interface (see Fig. 2 for the ranges of the examined properties). The cross-sectional vegetative blockage factor B_X (cf., Green 2006; Nikora et al. 2008) was computed from the surveyed two-stage geometry and the estimated vegetation height at different water levels. In addition, we determined the spatially-averaged vegetation properties of the 190 m long vegetated test reach by assuming that Grasses-N was representative of the areas outside the sub-reaches. For the analysis of mean annual deposition, we computed the maximum inundated vegetation height, dry mass, and C_DaH as a mean of the two-year data, assuming that the floodplain water depth of h=0.5 m was representative of the maximum water levels. In linear regression analyses, the strength of the regressions was assessed in terms of the correlation coefficient r (p<0.05 was considered as statistically significant).

Figure 2. Conceptualization of factors controlling the total flow resistance at overbank flows (n_{tot}), and the present study conditions. The two main components of n_{tot} are n_{veg} that includes the resistance factors related to the floodplain vegetation, and n_{base} that lumps the remaining factors. In the present case, n_{veg} contributed on average 89% of n_{tot}, and thus our analyses focus on the relationship between vegetative properties and n_{tot}.

Modeling concepts

This section presents the models used to describe the effect of the floodplain vegetation on the flow resistance and suspended sediment transport. The flow resistance coefficient (Manning's n) was computed for the sub-reaches and the entire test reach as

$$n = \frac{1}{u_m} KR^{2/3}S^{1/2} \qquad (2)$$

where R is the hydraulic radius (wetted area A divided by the wetted perimeter P), and K=1 $m^{1/3}/s$ is a constant. The cross-sectional mean velocity u_m was calculated as Q/A with Q obtained from the rating curve at the downstream station. The energy slope S was determined for the sub-reaches from the manual water level data, and for the entire test reach from the continuous data that was averaged for each autumn (Sep–Dec) and spring (Mar–May). The Manning coefficient of the main channel (n_{mc}) was obtained for the sub-reaches as the average of up to three values determined at water levels of 0–0.25 m below the floodplain level. At overbank flows, the various factors contributing to the total resistance (n_{tot}) are lumped into two resistance coefficients: n_{veg} generated by the floodplain vegetation, and n_{base} for the remaining factors (Fig. 2). n_{base} was obtained from overbank flow data of the entire test reach in spring 2010 when the floodplain was still completely bare. The shares of the total resistance generated by n_{veg} and n_{base} (see Fig. 2) were determined by assuming linear superposition of the corresponding stresses according to e.g. Yen (2002). Our analyses showed that the floodplain vegetation strongly dominated the total resistance, and thus we focused on the estimation of n_{tot}. The main source of error for n was the measured water surface slope, and the mean errors in head loss were estimated to be ±10 mm and ±4 mm for the test reach and the sub-reaches, respectively. With the mean head losses of 189 mm and 14.2 mm, the mean errors in n were estimated to be 3% and 14% for the test reach and the sub-reaches, respectively.

The data of the autumn 2011 allowed us to compute the dimensionless mean flow velocities within the vegetation (u^*_v) and in the unvegetated segment of the cross-section (u^*_0) with the model of Luhar and Nepf (2013):

$$u_0^* = \frac{u_0}{(gSH)^{1/2}} = \left(\frac{2P(1-B_X)}{C_f L_b + C_v L_v} \right)^{1/2} \quad (3)$$

$$u_v^* = \frac{u_v}{(gSH)^{1/2}} = \left(\frac{2PB_X + C_v L_v (u_0^*)^2}{C_D a P h B_X} \right)^{1/2} \quad (4)$$

where g is the gravitational acceleration, and C_f and C_v are the drag coefficients describing the bed stress and the shear stress at the interface between the vegetated floodplain and the main channel, respectively. L_b and L_v are the total lengths of the interfaces between the bed and the unvegetated flow, and between the vegetation and open water, respectively. The computed velocities u^*_v and u^*_0 were not validated as only the cross-sectional mean velocity was available from the field data. The shares of the discharge within the vegetation and in the unvegetated segment were obtained as $u^*_v B_X$ and $u^*_0(1-B_X)$, respectively. Luhar and Nepf (2013) found similar ranges for C_f ($0.015 \leq C_f \leq 0.19$) and C_v ($0.005 \leq C_v \leq 0.21$) from literature data. Thus, they assumed that for practical applications C_f=C_v=C*, where C* is a drag coefficient that lumps the bed and interfacial shear. In the present case, C* incorporates not only the main channel's bed shear, but also its distinct roughness elements, such as aquatic vegetation patches. C* of the test reach could be calibrated

from a simplified momentum balance (Eq. (5) below; Luhar and Nepf 2013) because $L_b + L_v \approx P$ in the two-stage geometry. The C^* value was derived at the lowest B_X separately for autumn (C^*=0.079, B_X=0.24) and spring (C^*=0.034, B_X=0.13) conditions by using the experimentally obtained n_{tot} and the spatially-averaged values of R and B_X. Further, we investigate the applicability of Eq. (5) to the vegetated two-stage channel by evaluating how reliably greater n_{tot} values at larger blockages (B_X up to 0.53) can be extrapolated from the known B_X and calibrated C^*. The performance of the model was assessed using the root mean square error and the Nash-Sutcliffe efficiency ($R_{eff} = 1 - \sum(n_{tot,mes,i} - n_{tot,pred,i})^2 / \sum(n_{tot,mes,i} - n_{tot,mes,mean})^2$ where $n_{tot,mes,i}$, $n_{tot,pred,i}$, and $n_{tot,mes,mean}$ refer to the ith measurement, the ith prediction, and the average of the measurements, respectively).

$$n_{tot}\left(\frac{g^{1/2}}{R^{1/6}}\right) = \left(\frac{C^*}{2}\right)^{1/2}\left(1 - B_X\right)^{-3/2} \qquad (5)$$

Eq. (5) neglects the flow within the vegetation, which Luhar and Nepf (2013) justified for dense aquatic vegetation (a≈100 m^{-1}) up to B_X≈0.7, when u^*_v is an order of magnitude lower than u^*_0. It follows that the general prerequisite for the validity of Eq. (5) is that $u^*_0(1-B_X)$>~0.8. The test reach fulfilled this prerequisite when using spatially-averaged variables (see Results and Discussion). The suspended sediment transport on the floodplain was examined by determining the distances over which flocs from the SS replenishment point (defined as the location where the SS stock of the floodplain is replenished through lateral advection from the main channel) are advected within vegetation before being deposited. The advection length scales were computed for flocs of the measured size distribution as (Zong and Nepf 2011)

$$x_a = u_v h / w_s \qquad (6)$$

where w_s is the particle settling velocity (m s^{-1}). The settling velocities were estimated from the relationship derived for cohesive suspended flocs of approximately similar size distribution as the present SS by Thonon et al. (2005): $w_s = 2.7\times10^{-7} D^{1.57}$, where D is the floc diameter in μm.

Results and discussion

Flow–vegetation interaction: vegetative properties for hydraulic modeling

In this section, we examine firstly the effect of the relative submergence on the flow resistance, and the dependence of the flow–vegetation interaction on the different vegetation properties (B_X, m_D, m_W, and $C_D a$). Subsequently, we investigate the flow resistance modeling in the two-stage context. Fig. 3a shows the average floodplain water depth of the five sub-reaches as a function of the discharge, illustrating the effect of the seasonally varying vegetative conditions (Fig. 3b). Fig. 3c plots the experimentally obtained Manning's n in the sub-reaches. The resistance coefficient of the small main channel (n_{mc}) varied between the sub-reaches and reached values above 0.1, because some sub-reaches had irregular geometry, fluffy bottom sediment,

298 woody debris, and some aquatic vegetation. In addition, notable seasonal variation occurred in n_{mc}. At
299 overbank flows (h>0 m), n_{tot} was clearly higher in autumn when the grasses were fresh and the willows
300 foliated as opposed to the following spring when the grasses were wilted and the willows leafless. The
301 resistance coefficient of the unvegetated channel (n_{base}, see Fig. 2) was 0.027–0.037 at the mean relative flow
302 depth (floodplain depth divided by total depth) of 0.25-0.53, i.e., at conditions ranging from low to almost
303 full submergence of the floodplain. Floodplain vegetation generated on average 89% of the total resistance
304 (see Fig. 2) as derived with the mean values of n_{tot}=0.088 from Fig. 3c and n_{base}=0.029. The share of the
305 vegetative resistance was 66% at low n_{tot}=0.05 and 80% at n_{tot}=0.065. Under such conditions where the
306 floodplain vegetation so strongly dominates the total resistance, n_{tot} may be used instead of methods based
307 on partitioning the cross-section.

308

309 **Figure 3. (a) Mean floodplain water depth of the sub-reaches as a function of discharge; (b) spatially-**
310 **averaged vegetative blockage factor in different seasons, (c) Manning's *n* of the sub-reaches at**
311 **overbank conditions (n_{tot}) and at bankful conditions of the main channel (n_{mc}); (d) n_{tot} as a function of**
312 **the relative submergence (the dashed line marks h/H=1).**

313 *Effect of the relative submergence on the flow resistance*

314 The resistance coefficient n_{tot} increased with increasing relative submergence up to h/H=1.0 (r=0.39,
315 p=0.045) and decreased at $1 \leq h/H \leq 3$ (r=0.67, p=0.025; Fig. 3d). The decrease was less pronounced than
316 that obtained experimentally by Wu et al. (1999) or theoretically by Luhar and Nepf (2013) for idealized
317 vegetation in a simple channel geometry. The difference against the earlier results was attributed to the fact
318 that the present two-stage channel with the vegetation having a non-homogeneous height distribution
319 differed from the simulated homogeneous vegetation. First, there was some floodplain vegetation
320 contributing to the flow resistance also at h/H>1.0 because of the selected definition of the vegetation height.
321 Second, the increasing water level resulted in more vegetation becoming inundated on the unexcavated bank,
322 which was not considered in the estimate of H. Third, H exhibited spatial variation within the sub-reaches
323 (see also Jalonen et al. 2014), and it is not fully solved how the representative vegetation height should be
324 determined under spatially variable conditions (cf., Green 2006). For $2 \leq h/H \leq 10$, there was no correlation
325 between n_{tot} and h/H (r=0.03, p=0.95; Fig. 3d), revealing that other factors controlled the flow resistance at
326 higher relative submergences. Wilson and Horritt (2002) compiled data for more homogeneous artificial and
327 natural grasses than in the current sub-reaches, and showed that the dependence of n_{tot} on the relative
328 submergence disappears at h/H >3…5. The overall scatter in the $n_{tot} - h/H$ plot (Fig. 3d) was mainly
329 attributed to the fact that different vegetation heights resulted in the same h/H but n_{tot} increased with the
330 increasing height for H>0.05 m (r=0.77, p<0.001) .

Dependence of the flow–vegetation interaction on B_X, m_D, m_W, and C_Da

Figs. 4a–c illustrate n_{tot} as a function of the inundated wet mass m_W and dry mass m_D, and the cross-sectional blockage factor B_X. Excluding the lowest blockages, n_{tot} showed a strong overall increase with B_X (r=0.78, p<0.001 for B_X>0.2). Exponential regressions for the different sub-reaches indicated that the grassy sub-reaches behaved similarly whereas the increase in n_{tot} with B_X was notably lower for the leafless and foliated willows. For the grasses, no notable differences in the $n_{tot} - B_X$ relationship were observed between the seasons or between the emergent (h/H<1.0) and submerged (h/H>1.0) conditions. The overall dependence of n_{tot} on m_D and m_W was weaker than for B_X even though the values represented a single season, which was related to the variation in C_Da between the sub-reaches (Fig. 5). With aH being linearly dependent on the dry mass (Eq. 1), the C_Da values indicated that a certain inundated mass corresponded to different height and blockage factor in Grasses-N and -D, explaining the variation in the regressions between these two sub-reaches (Figs. 4a–b). For Willows-M, C_Da in the layers above the grassy stubble (h>0.05 m) was an order of magnitude lower than for the grassy sub-reaches (Fig. 5).

The differences in C_Da between the sub-reaches caused the computed velocities within the vegetation (u^*_v in Eq. (4)) to be of the same order of magnitude than those of the unvegetated segment (u^*_0 in Eq. (3)) for the willows, whereas u^*_v was an order of magnitude lower than u^*_0 for the grassy sub-reaches. Thus, the sudden reduction in C_Da at the Willows-M and Bare-M sub-reaches enabled diverging flows from the main channel to the floodplain. The share of the discharge within the vegetation was on average 8% of the total for the grassy sub-reaches and 42% for the willows, and this difference was likely higher in the spring when the grasses were bent and the willows leafless. Thus, the grassy sub-reaches fulfilled the prerequisite for Eq. (5), which states that B_X is the only vegetation parameter needed to determine n_{tot} when the share of the discharge within the vegetation is less than 20% of the total. Similarly, the cross-sectional blockage factor is the main parameter for controlling the flow resistance of dense aquatic vegetation (e.g., Green 2006; Nikora et al. 2008). For the sparser willows, n_{tot} also depended on the parameter C_Da, and the low increase in n_{tot} with B_X was explained by the low C_Da values. In practice, with conventional methods a is more time-consuming and less accurate to obtain than inundated dry mass and vegetation height, but modern remote sensing methods, such as terrestrial laser scanning, are available for efficient collection of plant reference areas (e.g., Jalonen et al. 2015). From manually sampled vegetation, a can be derived for comparable floodplain grasses with Eq. (1).

Figure 4. n_{tot} as a function of (a) inundated wet vegetation mass; (b) inundated dry vegetation mass; (c) cross-sectional vegetative blockage factor (regressions for B_X>0.2). The lines denote exponential and linear regressions fitted for each sub-reach. In (c), the lower regression of Willows-M is for the leafless condition and the upper for the foliated condition. The symbols in (b) and (c) are same as in (a).

Figure 5. Total C_Da (markers connected with lines) and C_Da in 10-cm layers (filled markers without lines) as a function of vegetation height in autumn 2011.

For low values of the blockage factor (B_X=0–0.2), large scatter was observed in n_{tot} (Fig. 4c). The scatter reflected the differences in n_{mc} between the seasons and the sub-reaches (Fig. 3c) because n_{tot} was strongly dependent on n_{mc} at these low blockages (r=0.70, p =0.024 for B_X<0.2). Thus, it is important to take into account the main channel resistance when the vegetative blockage is low. In this two-stage geometry, B_X<0.2 was associated with either very low floodplain water level (h<0.05 m) or with h/H>2.3. Because the relative errors in n_{tot} increased with decreasing water surface slope, part of the scatter was likely caused by inaccuracy in the water level readings.

Modeling the flow resistance in the two-stage channel

The resistance coefficient n_{tot} of the 190 m long test reach was modelled with Eq. (5) using the C^* values calibrated at the lowest B_X separately for the spring and autumn conditions. The difference in C^* between autumn (C^*=0.079) and spring (C^*=0.034) was mainly attributed to the seasonal variation in the main channel vegetation which was not included in the determination of B_X. The C^* values were physically reasonable as they corresponded to n=0.036–0.048 and were thus somewhat higher than the resistance coefficient for the unvegetated conditions (n_{base}=0.029) where the interfacial shear stress was absent. In addition, our C^* values fell to the expected range for C_f ($0.015 \leq C_f \leq 0.19$) and C_v ($0.005 \leq C_v \leq 0.21$), and were close to the values ($0.05 \leq C^* \leq 0.13$) for simple channels with vegetated interfaces (Luhar and Nepf 2013). Fig. 6 shows the experimentally obtained (Eq. 2) and predicted (Eq. 5) n_{tot} in the different seasons at B_X=0.15–0.53 and h=0.1–0.7 m (Nash–Sutcliffe efficiency = 0.71; root mean squared error = 0.018). The prediction error was 17% in both autumns, 6% in spring 2011, and 15% in spring 2012. The greater error in autumn may be related to the fact that a certain relative bias in B_X causes a markedly higher error in n at greater values of B_X because of the power-type nature of Eq. (5). The model outcome can also be affected by the fact that the lowest B_X corresponded to the highest water level in the spring but to the lowest water level in the autumn. Although Eq. (5) is intended for submerged conditions characterized by interfacial shear above the vegetation, it produced satisfactory results for the emergent conditions as well. There was likely interfacial shear during the emergent flows because the majority of the grass blades were notably lower than the determined vegetation height, as indicated by the rapid decrease of C_Da in the 10-cm layers as the water level increased (Fig. 5). Overall, Eq. (5) performed well because the dense grassy floodplain cover dominated in the test reach, causing the discharge in the unvegetated segment to be more than 80% of the total in the spatially-averaged sense.

Figure 6. n_{tot} of the test reach: experimentally obtained vs. predicted with Eq. (5).

If woody vegetation had dominated the test reach, a notably higher density than in the Willows-M stand would have been necessary for Eq. (5) to be valid. According to Eqs. (3) and (4), the discharge within a *S.*

viminalis stand at B_X=0.5 would be less than 20% of the total if $C_D aH$>~1 ($C_D aH = C_{D\chi,F} A_L/A_B + C_{D\chi,S} A_S/A_B$, see Site and methodology). Thus, using Eq. (5) would require A_L/A_B>2.3 and A_S/A_B>0.33 for *S. viminalis* having a similar leaf-area-to-stem-area ratio as Willows-M (A_L/A_S=7). The required A_L/A_B and A_S/A_B are somewhat lower for those woody species that have higher drag coefficients (see Västilä and Järvelä 2014). A_L/A_B, i.e. leaf area index, of Willows-M (=0.25) was notably lower than for typical floodplain stands of deciduous woody vegetation, for which the mean A_L/A_B ranges at approximately 1–4 (Antonarakis et al. 2010; Forzieri et al. 2011). However, less than half of the foliage is typically located within the lowest few meters above the ground (Antonarakis et al. 2010). The woody parts of the present willows had a frontal area per volume of a=0.027 m^{-1} (corresponding to A_S/A_B=0.038 at H=1.3 m), which falls to the range recorded for willow shrubs and deciduous forests on floodplains (a=0.01–0.13 m^{-1}; Zinke 2011, and references therein).

Flow–vegetation–sediment interaction: erosion and deposition of cohesive matter

Fig. 7 shows the mean annual net deposition over the two-year period as a function of the maximum inundated vegetation height and dry mass. Net deposition exhibited a relationship to both vegetation properties, as indicated by the positive correlations obtained for all three investigated cross-sectional parts. The correlation was significant for the height on the inner floodplain and interface (r=0.71–0.74) and for the dry mass on the interface (r=0.73), but insignificant for the height on the bank (r=0.54) and for the dry mass on the inner floodplain and bank (r=0.18–0.62). In a study conducted in a gravel-bed river by Corenblit et al. (2009), the accretion of silt and sand within grassy to woody riparian vegetation was significantly correlated with the intercepted biovolume (which is analogous to the maximum inundated height as defined herein). The mean difference in the net deposition between the two cross-sections inside each sub-reach was 7 mm/a, which was expected to result mostly from measurement errors. Thus, we use the average net deposition of each sub-reach in the following analyses.

Figure 7. Mean annual net deposition (negative values refer to net erosion) in the three cross-sectional parts of the sub-reaches as a function of (a–c) maximum inundated vegetation height and (d–f) maximum inundated dry mass.

The average values revealed that net erosion occurred in all cross-sectional parts of Bare-M, deposition dominated in all parts of the grassy sub-reaches, and that Willows-M experienced both net deposition and erosion. According to Luhar et al. (2008), the shear-layer turbulence can penetrate to the bed of a submerged stand and re-suspend sediment only if $C_D aH$<0.23. In our sub-reaches, the lowest two-year mean $C_D aH$ values were obtained for Bare-M ($C_D aH$=0.19) and Willows-M ($C_D aH$=0.38). Thus, the low frontal area index of Bare-M led to re-suspension whereas the turbulent stresses were not able to reach the bed of Willows-M, which explained the greater tendency of Willows-M to deposition. These results were in line with the aH threshold derived by Luhar et al. (2008) from the experimental data of Moore (2004), which

shows that aquatic stands having aH>~0.4 can reduce SSC markedly more than stands having a lower aH. For the grassy sub-reaches, the range of $1.9 \leq C_D aH \leq 4.9$ explained the dominance of deposition.

The r values (Fig. 7) signified that the maximum inundated dry mass and height explained on average 32% and 45% of the deposition, respectively, which implied the presence of other controlling factors. The test reach formed a longitudinally extensive vegetated area, and under such conditions, deposition can be supply-limited (e.g., Sharpe and James 2006; Zong and Nepf 2011). In the present case, the SS stock on the inner floodplain was replenished in Bare-M and Willows-M through lateral advection by the diverging flows from the main channel. The manner in which the distance to the nearest such SS replenishment point affected the deposition can be illustrated by comparing the three grassy sub-reaches. In Grasses-U with the short distance of 15 m to the SS replenishment point (Bare M), the average deposition on the inner floodplain was above the fitted regression lines (Figs. 7b and e). By contrast, the average deposition on the inner floodplain was approximately equal to the expected value in Grasses-N and lower than expected in Grasses-D with the distances of 39 m and 73 m, respectively, to the nearest SS replenishment point (Willows-M). The advection length scales calculated for the representative case of u_v=0.01 m/s and H=0.2 m indicated that the largest 17–19% of the SS flocs were deposited before the flow entered the sub-reaches Grasses-N and -D under these hydraulic conditions. On the whole, the slightly better correlations for the height compared to the dry mass reflected the fact that the maximum inundated height increased the potential for deposition by increasing the advection length scale (Eq. 6) and the vegetative blockage. By contrast, as the velocity within the vegetation was mainly dependent on $(C_D a)^{-1/2}$, a higher $C_D aH$ and the associated higher dry mass limited the deposition in sub-reaches situated far from the SS replenishment point. In the present case, the differences in the explanative power of the height and dry mass were relatively low because of their strong correlation for the grassy vegetation.

In Grasses-N and -D, the average annual deposition was 8 mm or 64% lower on the inner floodplain compared to the interface although the vegetation properties differed by less than 20% between these cross-sectional parts. This finding indicated that most of the SS supplied to the interface via lateral diffusion from the main channel did not reach the inner floodplain. Thus, the present compound channel with the dense, often emergent vegetation did not follow the assumption that fine sediment deposits laterally uniformly across floodplains (Kronvang et al. 2009; Walling and He 1997). Flume experiments conducted by Sharpe and James (2006) under flow velocities and depths approximately representative of our field site confirm that lateral diffusion cannot effectively supply fine sediment to the inner floodplain. The strongest correlations between the deposition and vegetation properties were obtained for the interface having the least limited SS supply. However, the availability of SS at the interface slightly differed between the sub-reaches because of their differing inundation frequency and water depth. The Grasses-D that was inundated most often had a larger deposition at the interface than could be expected from the linear regressions. The difference was lower for Grasses-N that had on average 4 cm lower floodplain water depths, and negative for Grasses-U having on average 11 cm lower water depths.

Implications at the reach scale: focus on the cohesive sediment

Our field investigation showed that floodplain vegetation can significantly influence the flow hydraulics (e.g., Fig. 4) and cohesive sediment processes (Fig. 7), which has several implications at the reach scale. Vegetation increased Manning's *n* by up to fourfold depending on the season and water level, which highlighted the importance of reliable prediction of the vegetative flow resistance in the design and management of compound channels. The successful application of Eq. (5), illustrated in Fig. 6, indicated that it can be used to predict Manning's *n* in vegetated two-stage geometry. For instance, Eq. (5) allows determining how the vegetative blockage factor needs to be changed to reduce the flow resistance to a required level.

The designed bankful level provided high potential for deposition on the floodplain because the share of the SS load transported during overbank flows amounted to 90% of the total load in the wetter year and 70–80% in the drier year. In addition, overbank flows were typically characterized by notably higher SSC than the baseline value of 5–20 g/m^3 (as determined with the 1.2 μm filters). The spatially-averaged deposition on the 190 m long floodplain was 5.4 kg/m^2/a or 0.7 cm/m^2/a, which is of the same order of magnitude as for an agricultural floodplain in Denmark (0–6.3 kg/m^2/a, Kronvang et al. 2009) and for British floodplains (0.4–12.2 kg/m^2/a, Walling 1999). At the Ritobäcken, the total amount of trapped sediment may have been higher than indicated by the cross-sectional surveys because settling on vegetation surfaces can increase the removal of SS by up to 2 times depending on the horizontal plant area and the effect of the vegetation on the vertical turbulent mixing (e.g., Elliott 2000). The sediment deposited on the 190 m long floodplain comprised 3.4–5.5% of the total SS load, indicating that the floodplain was fairly stable. However, the results demonstrated the potential for obtaining either lower or higher deposition by controlling the properties of the plant stands. For instance, under supply-limited conditions, deposition can be easily increased by creating more SS replenishment points, i.e., short sparsely vegetated sub-reaches which allow the suspended sediment to be effectively distributed from the main channel to the floodplain. Under optimal supply conditions, the share of the deposited sediment was computed to increase almost linearly with the length of the two-stage reach.

The continuous data showed that the test reach underwent net deposition during the two-year period. However, the results did not preclude the possibility of seasonal erosion on the floodplain, similar to that caused by the growth and die-back of aquatic vegetation on channel beds (Cotton et al. 2006; Heppell et al. 2009), or minor net erosion in the main channel. Net deposition improved the water quality by reducing the turbidity and suspended sediment concentration of the water transported to downstream water courses. The matter deposited on the floodplain had a notable fraction of clay (17%), and 91% of the deposits consisted of particles finer than 58 μm. The D_{10}–D_{90} grain sizes of the suspended sediment were 2–5 times higher in the flocculated compared to the dispersed form. These figures are similar to those reported for large Dutch floodplains where aggregated flocs consisting of particles with a dispersed grain size of 2–35.4 μm constitute 90% of the deposited matter (Thonon et al. 2005).

In the investigated two-stage channel, the suspended sediment originates mainly from the catchment area (Västilä and Järvelä 2011), with the sub-surface drains of the fields expected to be a significant pathway, as is typical for agricultural sites with similar soils (e.g., Deasy et al. 2009; Warsta et al. 2013 and references therein). During the two-year monitoring, the annual mean SSC obtained with the 0.4 μm and 1.2 μm filters was 41 g/m^3 and 21 g/m^3, respectively, for the mean Q=0.08 m^3/s, and 54 g/m^3 and 34 g/m^3, respectively, for the mean Q=0.16 m^3/s. In channels receiving such high concentrations of SS and harmful sediment-bound substances, the two-stage approach allows reducing the loads of e.g. eutrophication-causing phosphorus or toxic heavy metals by managing the deposition of the cohesive fraction. Thus, a two-stage profile accompanied with suitable management of the floodplain vegetation can be employed e.g. in agricultural drainage for decreasing the input of phosphorus from fields to downstream water bodies. At the Ritobäcken, deposition typically occurred during rainfall-induced overbank flows in the autumn and spring, mainly at SSC=100–500 g/m^3 although such events covered only 2% of the time. The data confirmed that floodplain vegetation can enhance the water quality especially during high flows by reducing the peak concentrations of cohesive SS. Overall, our findings indicated that the transport of cohesive sediment can be controlled by two-stage designs.

Conclusions

Our field study provided knowledge and quantification on how flow and cohesive sediment processes in a two-stage channel depend on objectively measurable properties of the floodplain vegetation (relative submergence, height H, cross-sectional blockage factor B_X, dry mass, wet mass, C_Da, and distance from the suspended sediment replenishment point). The research was novel in showing that straightforward analyses together with a physically-based characterization of the plant stands can be used to describe the impact of floodplain vegetation in reach-scale engineering applications. The observed differences in the flow–vegetation interaction between the grasses and willows were explained by the parameter C_Da. The high vegetation density enabled the flow resistance of the grassy sub-reaches to be estimated primarily by the blockage factor whereas the results for the willows were indicative of the importance of C_Da for sparser woody vegetation. We found that the model based on B_X (Eq. (5)) was suitable for predicting the flow resistance in the grassycompound geometry, requiring the seasonal resistance changes controlled by sources other than floodplain vegetation to be calibrated at only one overbank condition. The parameter C_DaH was observed to characterize the tendency towards erosion or deposition while the magnitude of net deposition was most strongly explained by the maximum inundated vegetation height. Higher vegetation increased the availability of suspended sediment, with the results showing that deposition can be supply-limited even on such narrow floodplains if the vegetation is dense. As a practical implication, the two-stage approach was confirmed to provide potential for the management of fine sediment through appropriate maintenance of vegetation. The results of this research are expected to be useful for estimating the flow resistance and

deposition in compound channel designs that aim at reducing the adverse environmental effects associated with conventional channel engineering.

Acknowledgements

Financial support was received from the Academy of Finland (Grant No. 133113), Maa- ja vesitekniikan tuki ry, and the Ministry of Agriculture and Forestry. Help from Master's student Niina Siitonen, and the laboratory personnel at Aalto Water Engineering is acknowledged. We thank the Uusimaa Centre for Economic Development, Transport and the Environment, and Water Protection Association of the River Vantaanjoki and Helsinki Region for cooperation.

Notations

a	frontal area per unit volume (1/m)
A	wetted area
A_B	ground area (m^2)
A_L	leaf area (m^2)
A_S	stem area (m^2)
B_X	cross-sectional vegetative blockage factor (-)
C^*	bulk drag coefficient lumping the bed and interfacial shear (-)
C_D	drag coefficient (-)
$C_{D\chi,F}$	foliage drag coefficient (-)
$C_{D\chi,S}$	stem drag coefficient (-)
C_f	drag coefficient of the bed (-)
C_v	drag coefficient at the interface between vegetation and open water (-)
D	floc diameter (μm)
g	gravitational acceleration (m/s^2)
H	vegetation height (m)
h	water depth on the floodplain (m)

566	h/H	relative submergence (-)
567	K	constant of Eq. (2) ($m^{1/3}/s$)
568	L_b	total length of the interface between the bed and the open water (m)
569	L_v	total length of the interface between the vegetation and the open water (m)
570	m_D	dry vegetation mass (kg/m^2)
571	m_W	wet vegetation mass (kg/m^2)
572	n_{base}	Manning's resistance coefficient of the unvegetated channel at overbank flows (-)
573	n_{mc}	Manning's resistance coefficient at bankful flows (-)
574	n_{tot}	total Manning's resistance coefficient at overbank flows (-)
575	n_{veg}	Manning's resistance coefficient of the floodplain vegetation
576	P	wetted perimeter (m)
577	Q	discharge (m^3/s)
578	R	hydraulic radius (m)
579	S	energy slope (-)
580	SS	suspended sediment
581	SSC	suspended sediment concentration (g/m^3)
582	T	turbidity (NTU)
583	u_m	cross-sectional mean velocity (m/s)
584	u_v	velocity within vegetation (-)
585	u^*_v	dimensionless velocity within vegetation (-)
586	u_0	velocity in the unvegetated segment of the cross-section (-)
587	u^*_0	dimensionless velocity in the unvegetated segment of the cross-section (-)
588	x_a	advection length scale (m)
589	w_s	particle settling velocity (m/s)

References

Aberle, J., and Järvelä, J. (2013). "Flow resistance of emergent rigid and flexible floodplain vegetation." *J. Hydraul. Res*., 51(1), 33–45.

Antonarakis, A. S., Richards, K. S., Brasington, J., and Muller, E. (2010), "Determining leaf area index and leafy tree roughness using terrestrial laser scanning." *Water Resour. Res*., 46, W06510. doi:10.1029/2009WR008318.

Assselman, N. E. M, and van Wijngaarden, M. (2002). "Development and application of a 1D floodplain sedimentation model for the River Rhine in The Netherlands." *J. Hydrol*., 268(1–4), 127–142. doi: 10.1016/S0022-1694(02)00162-2.

Bilotta, G. S., and Brazier, R. E. (2008). "Understanding the influence of suspended solids on water quality and aquatic biota." *Water Res*. 42(12): 2849–2861.

Corenblit, D., Steiger, J., Gurnell, A. M., Tabacchi, E., and Roques, L. (2009). "Control of sediment dynamics by vegetation as a key function driving biogeomorphic succession within fluvial corridors." *Earth Surf. Process. Landforms*, 34, 1790–1810. doi: 10.1002/esp.1876.

Cotton, J. A., Wharton, G., Bass, J. A. B., Heppell, C. M., and Wotton, R. S. (2006). "The effects of seasonal changes to in-stream vegetation cover on patterns of flow and accumulation of sediment." *Geomorphology*, 77(3–4), 320–334. doi: 10.1016/j.geomorph.2006.01.010.

Deasy, C., Brazier, R. E., Heathwaite, A. L., and Hodgkinson, R. (2009). "Pathways of runoff and sediment transfer in small agricultural catchments." *Hydrol. Process.*, 23, 1349–1358. doi: 10.1002/hyp.7257.

DEFRA (2004). *Reducing uncertainty in river flood conveyance, Phase 2: Conveyance Manual*. Environment Agency, Bristol.

De Doncker, L., Troch, P., Verhoeven, R., Bal, K., Desmet, N., and Meire, P. (2009). "Relation between resistance characteristics due to aquatic weed growth and the hydraulic capacity of the river Aa." *River Res. Applic.*, 25, 1287–1303. doi: 10.1002/rra.1240.

DVWK. (1991). "Hydraulische Berechnung von Fliessgewässern." DVWK Merkblätter zur Wasserwirtschaft, 0722-7167; 220. Parey: Hamburg. ISBN: 3-490-32097-2.

Elliott, A. H. (2000). "Settling of fine sediment in a channel with emergent vegetation." *J. Hydraul. Eng*., 126(8), 570–577.

Forzieri, G., Degetto, M., Righetti, M., Castelli, F., and Preti, F. (2011). "Satellite multispectral data for improved floodplain roughness modelling," *J. Hydrol.*, 407(1–4), 41–57. doi: 10.1016/j.jhydrol.2011.07.009.

Geerling, G. W., Kater, E., van den Brink, C., Baptist, M. J., Ragas, A. M. J., and Smits, A. J. M. (2008). "Nature rehabilitation by floodplain excavation: The hydraulic effect of 16 years of sedimentation and vegetation succession along the Waal River, NL." *Geomorphology*, 99(1–4), 317–328.

623 Green, J. C. (2006). “Effect of macrophyte spatial variability on channel resistance.” *Adv. Water Resour*., 29,
624 426–438.

625 Helmiö, T., and Järvelä, J. (2004). ”Hydraulic aspects of environmental flood management in boreal
626 conditions.” *Boreal Env. Res.*, 9(3), 227–241.

627 Heppell, C. M., Wharton, G., Cotton, J. A. C., Bass, J. A. B., and Roberts, S. E. (2009). “Sediment storage in
628 the shallow hyporheic of lowland vegetated river reaches.” *Hydrol. Process.*, 23, 2239–2251. doi:
629 10.1002/hyp.7283.

630 Hey, R. D. (2009). “Environmentally sensitive river engineering.” *The Rivers Handbook: Hydrological and*
631 *Ecological Principles, Volume Two*, P. Calow and G. E. Petts, eds., Blackwell Science Ltd, Oxford, UK.,
632 337–362. doi: 10.1002/9781444313871.ch18.

633 Huai, W., Gao, M., Zeng, Y., and Li, D. (2009). “Two-dimensional analytical solution for compound channel
634 flows with vegetated floodplains.” *Appl. Math. Mech. -Engl. Ed*., 30(9), 1121–1130. doi: 10.1007/s10483-
635 009-0906-z.

636 Jalonen, J., and Järvelä, J. (2014). “Estimation of drag forces caused by natural woody vegetation of different
637 scales.” *J. Hydrodyn.*, 26, 608–623. doi: 10.1016/S1001-6058(14)60068-8.

638 Jalonen, J., Järvelä, J., Koivusalo, H., and Hyyppä, H. (2014). “Deriving floodplain topography and
639 vegetation characteristics for hydraulic engineering applications by means of terrestrial laser scanning.” *J.*
640 *Hydraul. Eng.*, 140, doi:10.1061/(ASCE)HY.1943-7900.0000928.

641 Jalonen, J., Järvelä, J., Virtanen, J.-P., Vaaja, M., Kurkela, M., and Hyyppä, H. (2015). Determining
642 characteristic vegetation areas by terrestrial laser scanning for floodplain flow modeling. *Water*, 7(2), 420-
643 437. doi: 10.3390/w7020420

644 Kang, H., and Choi, S-U. (2006). “Turbulence modeling of compound open-channel flows with and without
645 vegetation on the floodplain using the Reynolds stress model.” *Adv. water res*., 29, 1650–1664.

646 Knight, D. W., Tang, X., Sterling, M., Shiono, K., and McGahey., C. (2010). “Solving open channel flow
647 problems with a simple lateral distribution model.” *River Flow 2010,* Dittrich, A., Koll, Ka., Aberle, J., and
648 Geisenhainer, P.,eds, Bundesanstalt für Wasserbau, Karlsruhe, 41-48. ISBN 978-3-939230-00-7.

649 Kronvang, B., Hoffmann, C. C., and Dröge, R. (2009). “Sediment deposition and net phosphorus retention in
650 a hydraulically restored lowland river floodplain in Denmark: combining field and laboratory experiments.”
651 *Mar. Freshwater Res*., 60, 638–646.

652 Kouwen, N., and Unny, T. E. (1973). “Flexible roughness in open channels”. *Journal of the Hydraulics*
653 *Division, Proceedings of the American Society of Civil Engineers*, 99(HY5), 713–728.

654 Luhar, M., Rominger, J., and Nepf, H. (2008). “Interaction between flow, transport and vegetation spatial
655 structure.” *Environ. Fluid Mech.*, 8, 423–439.

656 Luhar, M., and Nepf, H. (2013). “From the blade scale to the reach scale: A characterization of aquatic
657 vegetative drag.” *Adv. Water Resour*., 51, 305–316. doi:10.1016/j.advwatres.2012.02.002.

658 Moore, K. A. (2004). “Influence of seagrasses on water quality in shallow regions of the lower Chesapeake
659 Bay.” *J. Coast. Res.*, 20, 162–178.

660 Myers, W. R., and Lyness, J. F. (1994). “Hydraulic study of a two-stage channel.” *Regul. river*, 9: 225-235.

661 Nikora, V., Larned, S., Nikora, N., Debnath, K., Cooper, G., and Reid, M. (2008). “Hydraulic resistance due
662 to aquatic vegetation in small streams: field study.” *J. Hydraul. Eng*., 134(9), 1326–1332.

663 Owens, P. N., Batalla, R. J., Collins, A. J., Gomez, B., Hicks, D. M., Horowitz, A. J., Kondolf, G. M.,
664 Marden, M., Page, M. J., Peacock, D. H., Petticrew, E. L., Salomons, W., and Trustrum, N. A. (2005). “Fine-
665 grained sediment in river systems: environmental significance and management issues.” *River Res. Applic*.,
666 21, 693–717. doi: 10.1002/rra.878

667 Powell, G. E., Ward, A. D., Mecklenburg, D. E., Draper, J., and Word, W. (2007). “Two-stage channel
668 systems: Part 2, case studies.” *J. Soil Water Conserv.*, 62(4): 286–296.

669 Sellin, R. H. J., Giles, A., and van Beesten, D. P. (1990). “Post-Implementation Appraisal of a Two-Stage
670 Channel in the River Roding, Essex.” *Water and Env. J.*, 4, 119–130. doi: 10.1111/j.1747-
671 6593.1990.tb01567.x.

672 Sharpe, R. G., and James, C. S. (2006). “Deposition of sediment from suspension in emergent vegetation.”
673 *Water SA*, 32(2), 211–218.

674 Thonon, I., Roberti, J. R., Middelkoop, H., van der Perk, M., and Burrough, P. A. (2005). “In situ
675 measurements of sediment settling characteristics in floodplains using a LISST-ST.” *Earth Surf. Process.*
676 *Landforms*, 30, 1327–1343. doi: 10.1002/esp.1239.

677 Thornton, C. I., Abt, S. R., and Clary, W. P. (1997). “Vegetation influence on small stream siltation.” *J. Am.*
678 *Water Resour. As.*, 33(6), 1279–1288.

679 USDA (2007). “Two-Stage Channel Design”. In: *National Engineering Handbook, Part 654 Stream*
680 *Restoration Design*. Natural Resources Conservation Service.

681 Västilä, K., and Järvelä, J. (2011). ”Environmentally preferable two-stage drainage channels: considerations
682 for cohesive sediments and conveyance.” *Int. J. River Basin Manage.*, 9(3-4): 171–180. doi:
683 10.1080/15715124.2011.572888.

684 Västilä, K., and Järvelä, J. (2014). ”Modeling the flow resistance of woody vegetation using physically-
685 based properties of the foliage and stem.” *Water Resour. Res.*, 50, 229–245, doi: 10.1002/2013WR013819.

686 Walling, D. E., and He, Q. (1997). “Investigating spatial patterns of overbank sedimentation on river
687 floodplains.” *Water Air Soil Poll*., 99, 9–20.

688 Walling, D. E. (1999). “Linking land use, erosion and sediment yields in river basins.” *Hydrobiologia*, 410,
689 223–240.

690 Warsta, L., Taskinen, A., Koivusalo, H., Paasonen-Kivekäs, M., and Karvonen, T. (2013). “Modelling soil
691 erosion in a clayey, subsurface-drained agricultural field with a three-dimensional FLUSH model.” *J.*
692 *Hydrol.*, 498, 132–143. doi: 10.1016/j.jhydrol.2013.06.020.

693 Wilson, C. A. M. E., and Horritt, M. S. (2002). “Measuring the flow resistance of submerged grass.” *Hydrol.*
694 *Process*., 16, 2589–2598. doi: 10.1002/hyp.1049.

695 Wu, F., Shen, H., and Chou, Y. (1999). ”Variation of roughness coefficients for unsubmerged and
696 submerged vegetation.” *J. Hydraul. Eng*., 125(9), 934–942.

697 Yang, K., Liu, X., Cao, S., and Huang, E. (2014). “Stage-discharge prediction in compound channels.” *J.*
698 *Hydraul. Eng*., 140(4), 06014001. doi: 10.1061/(ASCE)HY.1943-7900.0000834.Yen, B. C. (2002). “Open
699 channel flow resistance.” *J. Hydraul. Eng.*, 128, 20-39.

700 Zinke, P. (2011). “Modelling of flow and levee depositions in a freshwater delta with natural vegetation.”
701 Doctoral thesis. Faculty of Civil Engineering, Norwegian University of Science and Technology.

702 Zong, L., and Nepf, H. (2011). “Spatial distribution of deposition within a patch of vegetation.” *Water*
703 *Resour. Res*., 47, W03516. doi:10.1029/2010WR009516.

Figure1
Click here to download Figure: Figure1.tif

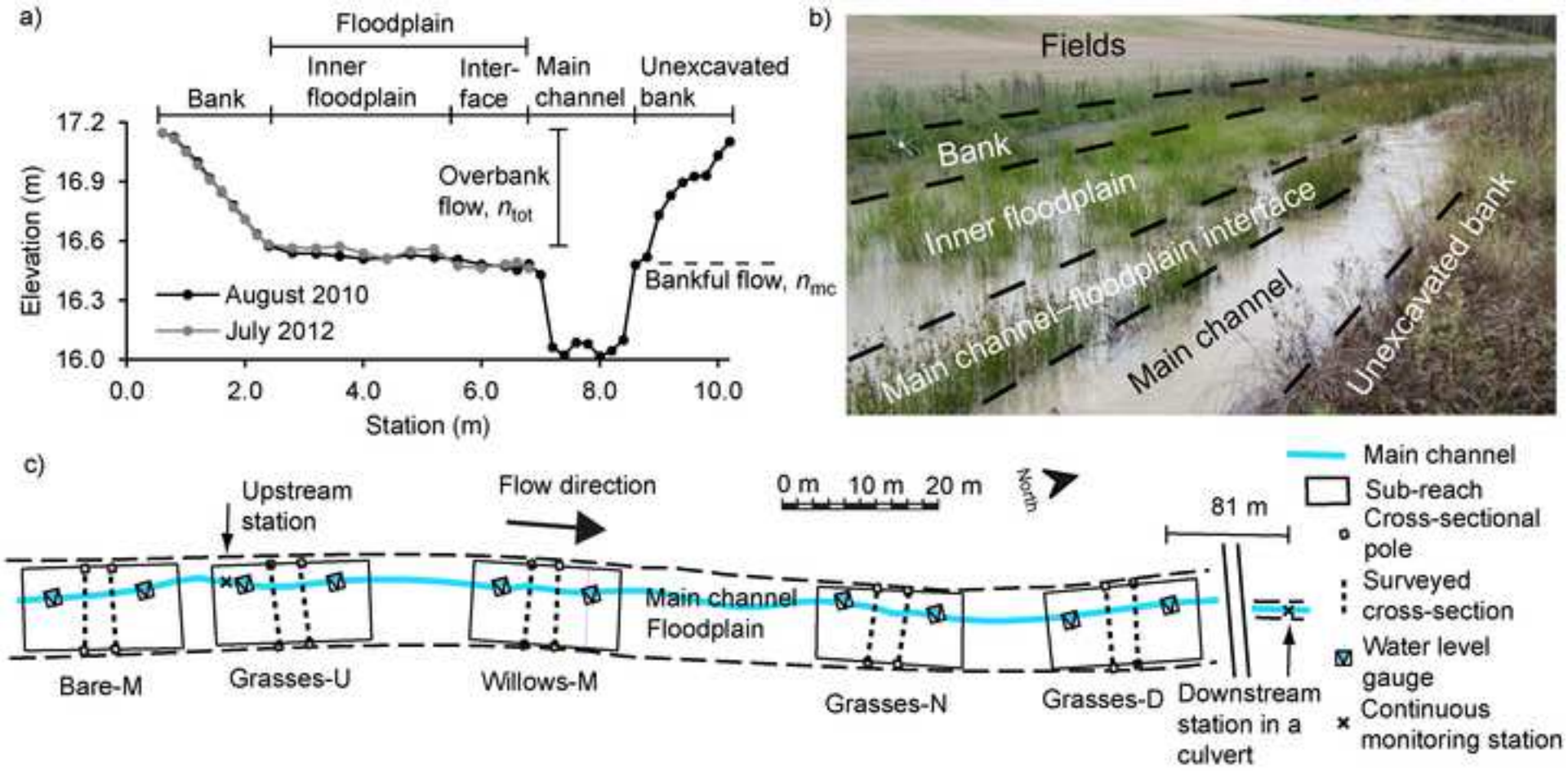

Figure2
Click here to download Figure: Figure2.eps

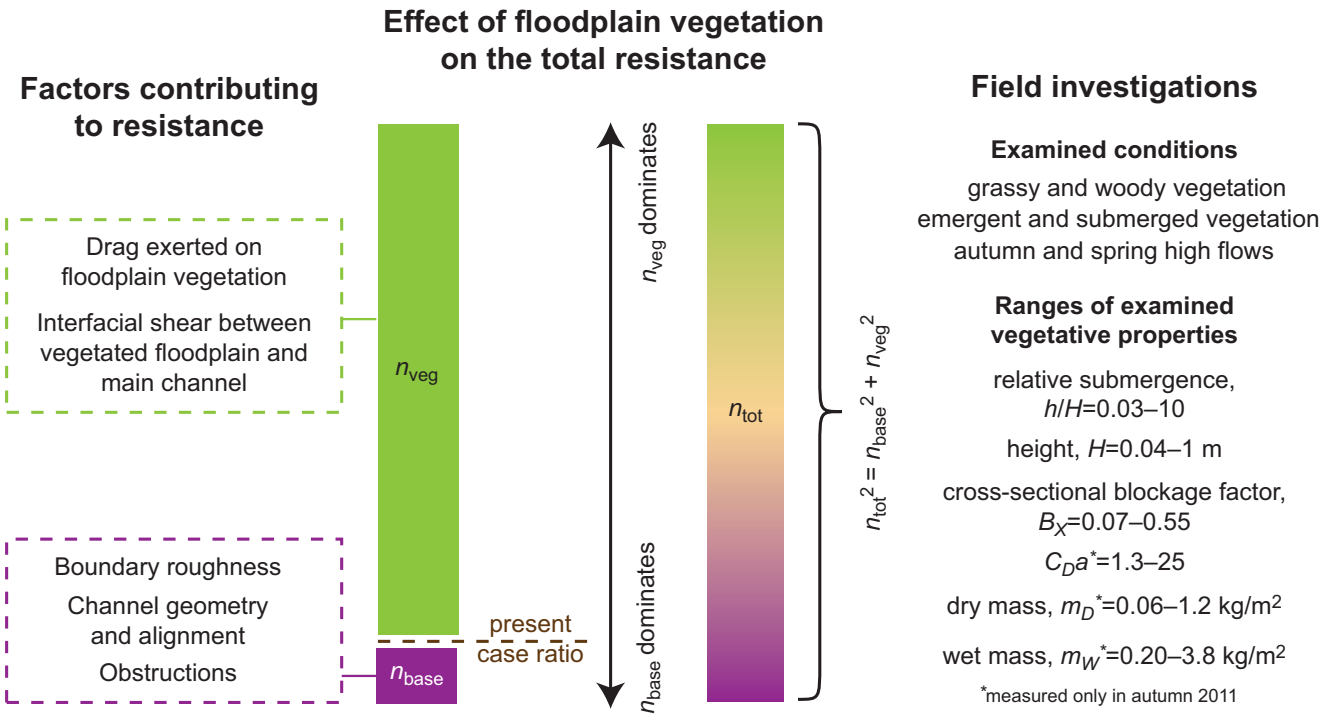

Figure3
Click here to download Figure: Figure3.eps

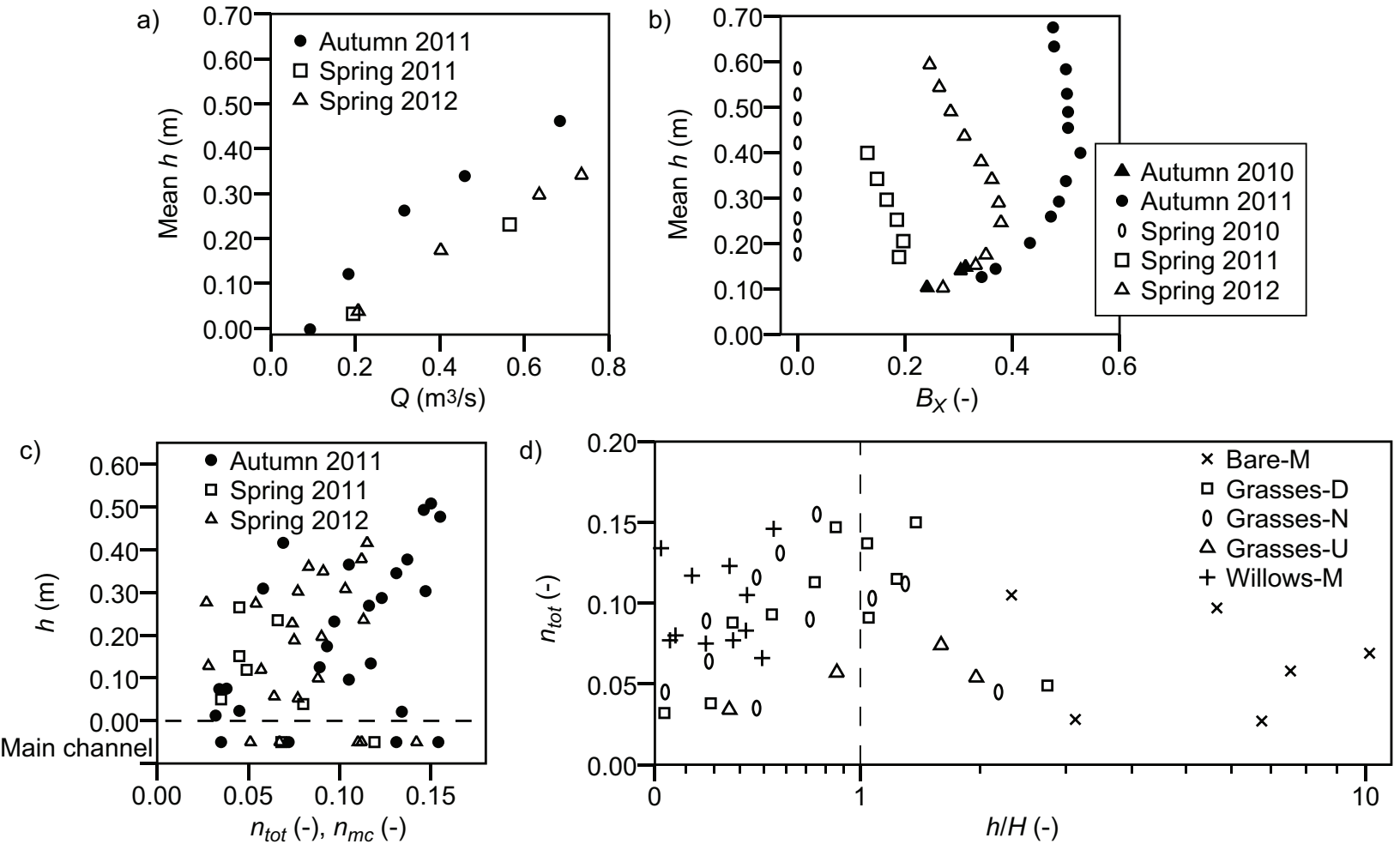

Figure4
Click here to download Figure: Figure4.eps

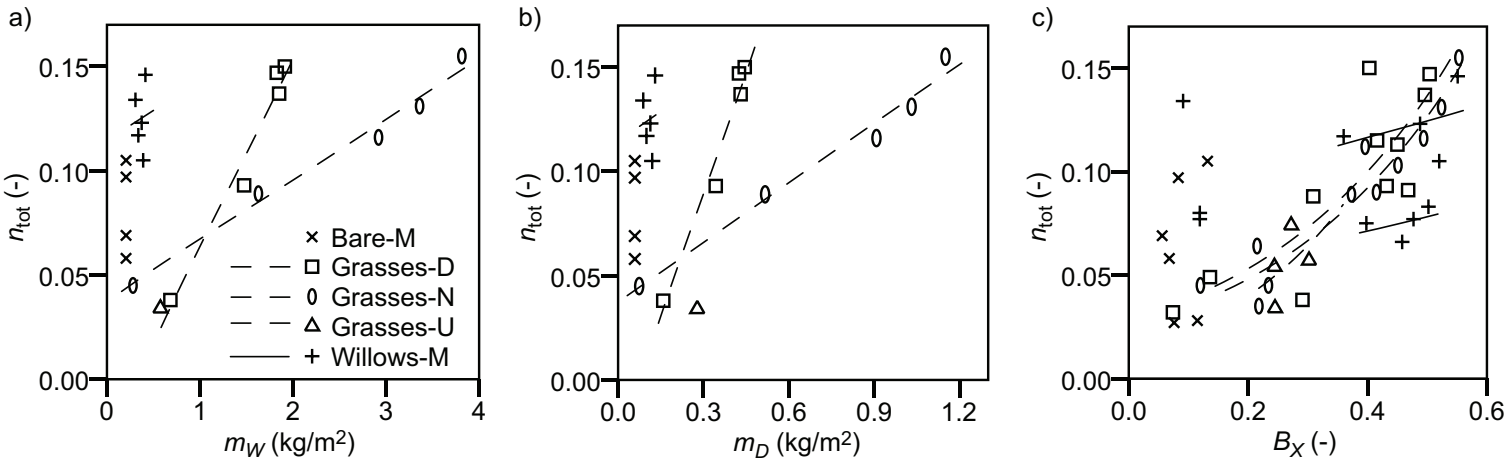

Figure5
Click here to download Figure: Figure5.eps

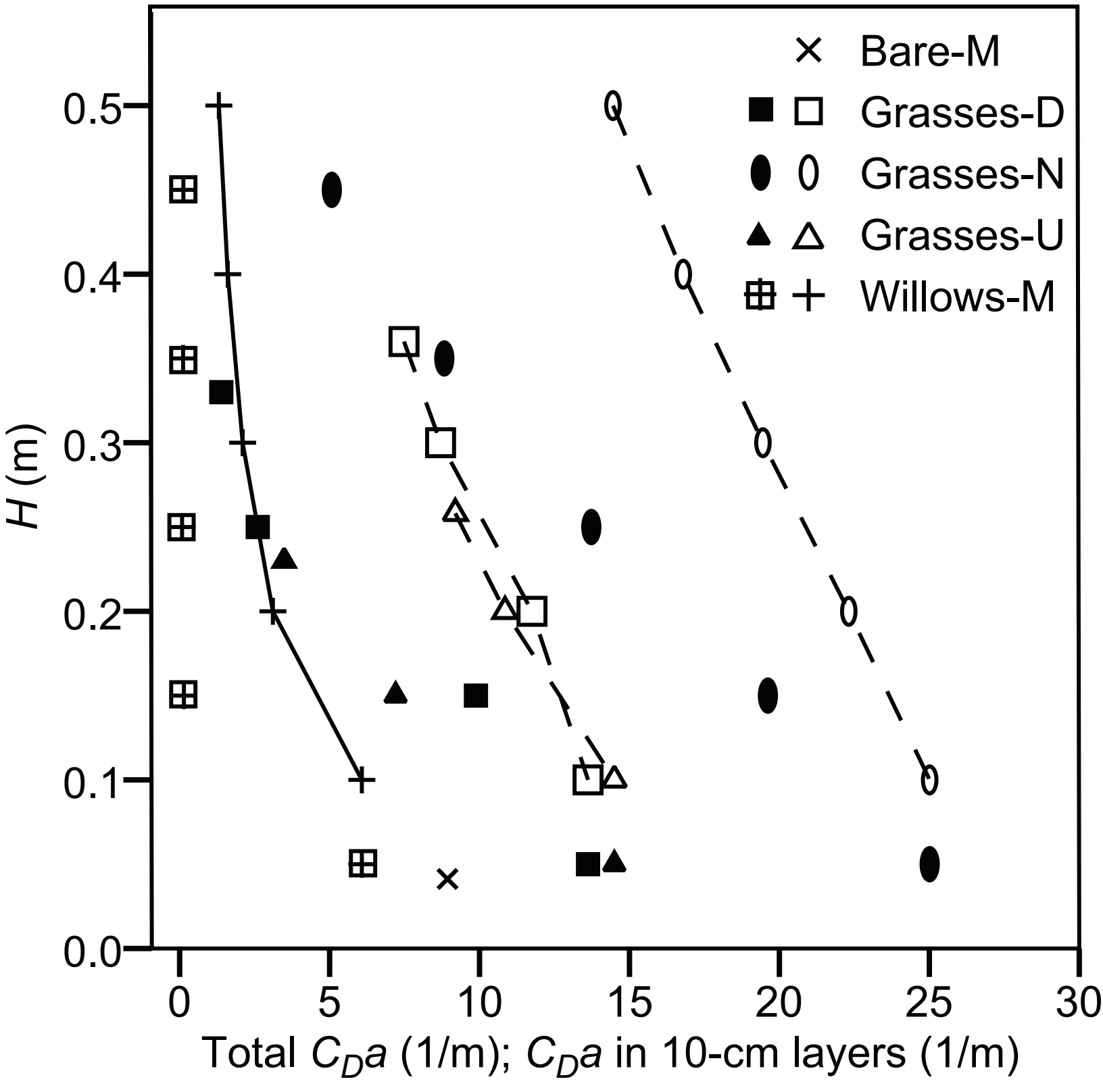

Figure6
Click here to download Figure: Figure6.eps

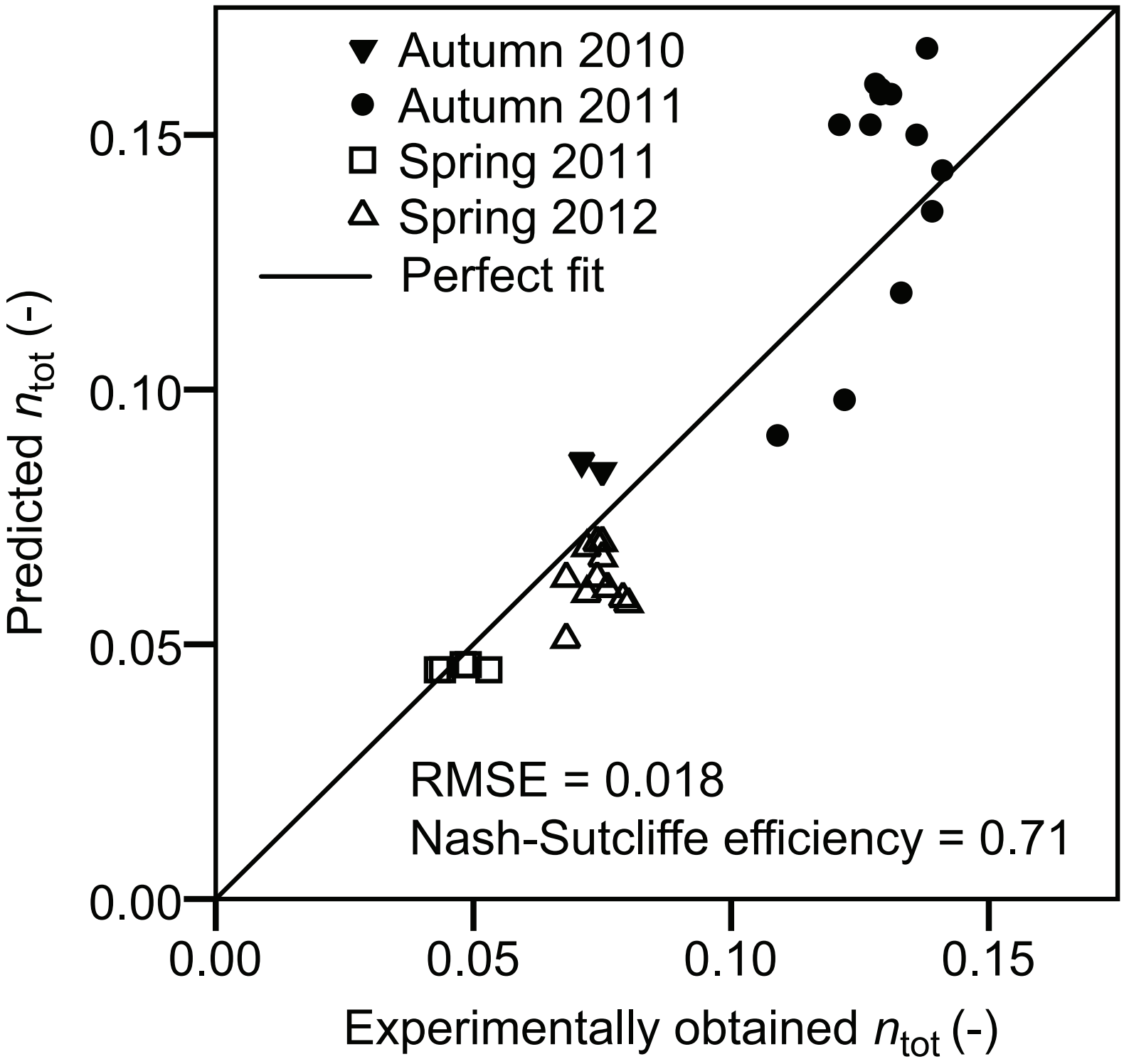

Figure7
Click here to download Figure: Figure7.eps

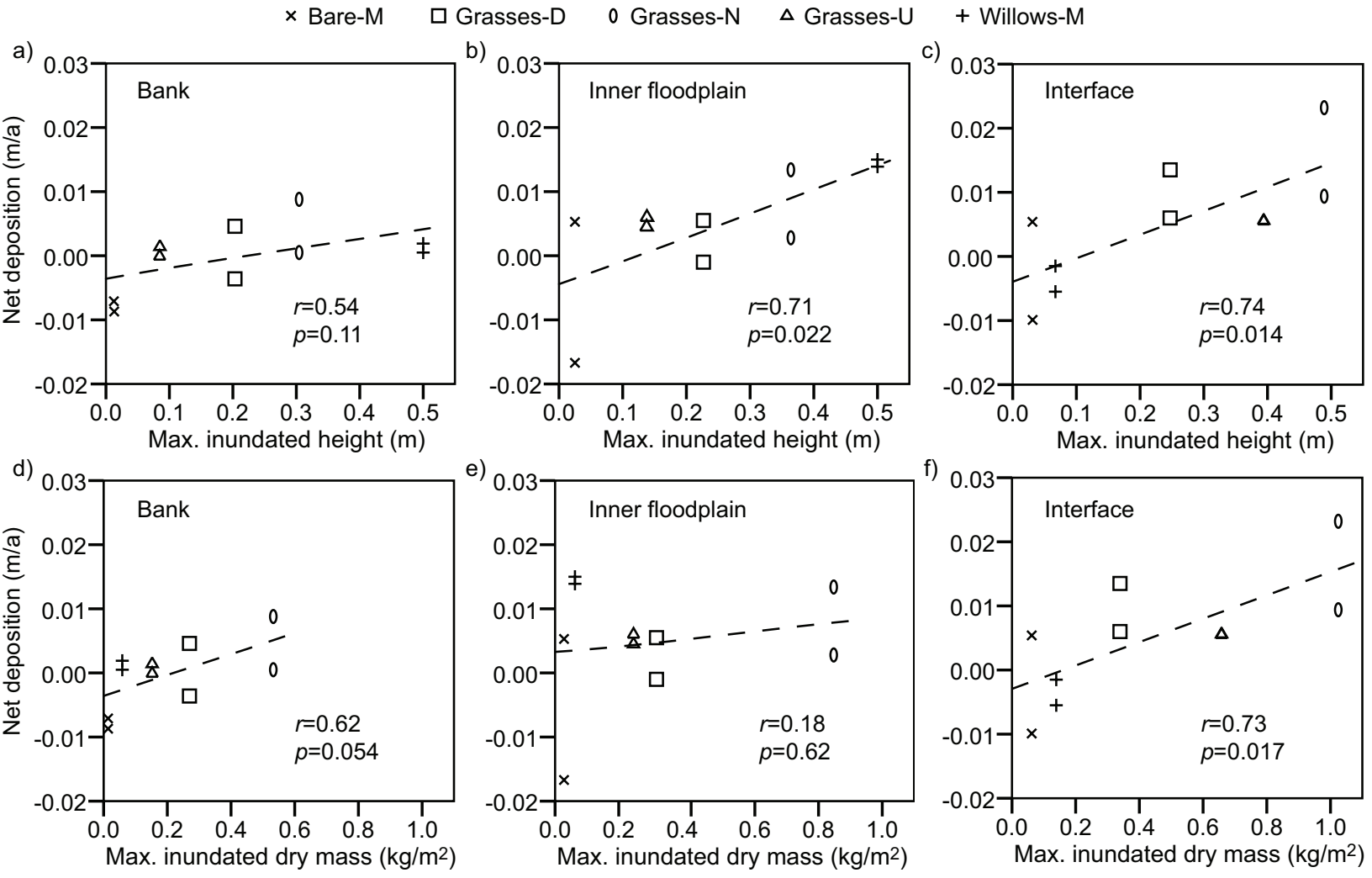

Figure Caption List

Figure 1. (a) A representative two-stage cross-section with the surveyed geometry in 2010 and 2012; (b) the test reach at a low floodplain water depth; (c) the field site with the monitoring infrastructure.

Figure 2. Conceptualization of factors controlling the total flow resistance at overbank flows (n_{tot}), and the present study conditions. The two main components of n_{tot} are n_{veg} that includes the resistance factors related to the floodplain vegetation, and n_{base} that lumps the remaining factors. In the present case, n_{veg} contributed on average 89% of n_{tot}, and thus our analyses focus on the relationship between vegetative properties and n_{tot}.

Figure 3. (a) Mean floodplain water depth of the sub-reaches as a function of discharge; (b) spatially-averaged vegetative blockage factor in different seasons, (c) Manning's n of the sub-reaches at overbank conditions (n_{tot}) and at bankful conditions of the main channel (n_{mc}); (d) n_{tot} as a function of the relative submergence (the dashed line marks h/H=1).

Figure 4. n_{tot} as a function of (a) inundated wet vegetation mass; (b) inundated dry vegetation mass; (c) cross-sectional vegetative blockage factor (regressions for B_X>0.2). The lines denote exponential and linear regressions fitted for each sub-reach. In (c), the lower regression of Willows-M is for the leafless condition and the upper for the foliated condition. The symbols in (b) and (c) are same as in (a).

Figure 5. Total C_Da (markers connected with lines) and C_Da in 10-cm layers (filled markers without lines) as a function of vegetation height in autumn 2011.

Figure 6. n_{tot} of the test reach: experimentally obtained vs. predicted with Eq. (5).

Figure 7. Mean annual net deposition (negative values refer to net erosion) in the three cross-sectional parts of the sub-reaches as a function of (a–c) maximum inundated vegetation height and (d–f) maximum inundated dry mass.